Elasticity and plasticity in stiff and flexible oligomeric glasses

Oleg Gendelman,[1] H. George E. Hentschel,[2] Pankaj K. Mishra,[3] Itamar Procaccia,[3] and Jacques Zylberg[3]
[1]*Faculty of Mechanical Engineering, Technion - Israel Institute of Technology, Haifa, Israel*
[2]*Department of Physics, Emory University, Atlanta, Georgia, USA*
[3]*Department of Chemical Physics, Weizmann Institute of Science, Rehovot 76100, Israel*
(Received 4 July 2014; published 30 October 2014)

In this paper we focus on the mechanical properties of oligomeric glasses (waxes), employing a microscopic model that provides, via numerical simulations, information about the shear modulus of such materials, the failure mechanism via plastic instabilities, and the geometric responses of the oligomers themselves to a mechanical load. We present a microscopic theory that explains the numerically observed phenomena, including an exact theory of the shear modulus and of the plastic instabilities, both local and system spanning. In addition we present a model to explain the geometric changes in the oligomeric chains under increasing strains.

DOI: 10.1103/PhysRevE.90.042315 PACS number(s): 64.70.pj

I. INTRODUCTION

A polymer is a macromolecule that consists of a large number of monomer subunits [1]. Polymeric glasses are solids composed of a large number of such polymeric units. Subjected to homogeneous strain such solids can exhibit a variety of interesting phenomena including crazing instabilities, shear banding, strain hardening, etc. [2]. Considerable effort was expended to describe these phenomena on the microscopic level using theory and simulations [3–5]. Under tensile strains cavities may nucleate in a hitherto homogeneous polymeric glass. It was argued that the formation of cavities takes place in regions of local low elastic modulus [6]. Polymeric glasses subjected to large strains exhibit strain hardening; this may suppress strain localization and consequent crazing, necking, shear banding, etc. Strain hardening is presumably caused by ordering the polymer beyond a certain strain threshold. The microscopic origin of strain hardening was studied using molecular dynamic simulations in Refs. [7,8], finding that the origin of this phenomenon is related to plastic rearrangements of the monomers. This also leads to short-range ordering. In spite of the above mentioned efforts a first-principles theory of these interesting phenomena is still incomplete. In particular in this paper we propose a microscopic theory that relates macroscopic observables with the conformational deformation of the oligomers under pure shear.

In recent years there has been great progress in understanding the mechanical properties of amorphous solids from first principles [9–11]. This progress was based on identifying elementary plastic events as the loss of mechanical stability when a Hessian eigenvalue hits zero [9–11]. This event is connected to a saddle node bifurcation in the generalized energy landscape. It was demonstrated also that these elementary events can aggregate and concatenate to yield shear localization and eventually shear bands [12,13]. The aim of this paper is to extend this analytic approach to plasticity from simple Lennard-Jones glasses (and recently some glasses with magnetic properties) [14–16] to the realm of short oligomeric (or wax) glasses. These are amorphous solids whose constituents are short chains of the order of 10–30 monomers, where the full impact of polymeric entanglement is still not crucial [17]. Nevertheless the existence of fairly long chains of connected monomers introduces a hierarchy of new length scales and energy scales related to valence bonds, valence angles, and interoligomer interactions. In particular the persistence length ℓ_p of the oligomer turns out to be crucial. Thus a variety of new phenomena and questions arise, calling for a careful numerical simulation and analytic assessment. Among the issues arising we will provide a microscopic theory for the shear modulus of these materials, for the failure mechanism through plasticity (both local and system spanning) and shed light on the geometric characteristic of the oligomers under mechanical yield.

The outline of the paper is as follows: In Sec. II we describe the atomistic model used in further simulations. The model employs Lennard-Jones, angular, and FENE interactions (see below for details). Section III presents first the results of numerical simulations for the stress versus strain curves, the energy budget, characteristics of the oligomeric chains like end-to-end distance, etc. For analytic transparency we perform the simulation in quasistatic athermal conditions to highlight the plastic events without any thermal fluctuations or strain rate effects that mask the fundamental physics. The same section provides some theory of these characteristics. In Sec. IV we present a theory for elementary plastic events. Next in Sec. V we discuss the failure mechanism involving shear localization and eventually shear bands. Section VI presents the analytic calculation of the shear modulus and a comparison with the numerics.

II. DESCRIPTION OF THE MODEL

We consider a system composed of N_p chains each comprising n monomers (oligomers). Thus the total number of particles in our system is $N = N_p \times n$. The interaction between monomers belonging to the same or to different oligomers is different. Interoligomer interactions are simply given by a truncated and smoothed Lennard-Jones potential $\phi_{\rm LJ}$; see below in Eq. (3). Within a given oligomer the interactions have three contributors. First, all monomers within the Lennard-Jones cutoff range $r_{\rm co}$ exert a force on each other which is derived from the potential $\phi_{\rm LJ}$. Second, a contribution χ is added to the energy of any two successive monomers within the polymer (to mimic the valence bond interaction). The third contribution to the energy is an angular potential to constrain the value of the valence angle θ determined by three

TABLE I. The parameters used in the simulation.

a	b	c0	c2	c4	c6	η	r_0	$\varphi^{\rm eq}$
3.9435	−3.892 68	1.2×10^{-3}	−0.0207	0.106 91	−0.143 794	30	1.5	π

successive monomers within a oligomer. This interaction is denoted below $\psi(\theta)$. Thus the total energy can be written as [18]

$$U = U^{\rm LJ} + U^{\rm FENE} + U^{\rm Angle}, \tag{1}$$

$$U^{\rm LJ} = \sum_{\langle ij\rangle}^{N} \phi_{\rm LJ}^{ij}, \quad U^{\rm FENE} = \sum_{k=1}^{N_p}\sum_{i=1}^{n-1} \chi_k^{i,i+1}, \tag{2}$$
$$U^{\rm Angle} = \sum_{k=1}^{N_p}\sum_{i=2}^{n-1} \psi_k^{i-1,i,i+1}.$$

The notation is such that successive particles are i and $i+1$ within a oligomer chain, and ψ_k^i stands for the angular contribution formed by any three successive particles $(i-1,i,i+1)$ within the k'th oligomer where i is the vertex.

The truncated and smoothed potential Lennard-Jones potential is defined as

$$\phi_{\rm LJ}^{ij} = 4\varepsilon\left[\left(\frac{\lambda}{r_{ij}}\right)^{12} - \left(\frac{\lambda}{r_{ij}}\right)^{6}\right], \quad r_{ij} \leqslant r_{\rm min}, \tag{3}$$

$$\phi_{\rm LJ}^{ij} = \varepsilon\left[a\left(\frac{\lambda}{r_{ij}}\right)^{12} - b\left(\frac{\lambda}{r_{ij}}\right)^{6} + \sum_{\ell=0}^{3} c_{2\ell}\left(\frac{r_{ij}}{\lambda}\right)^{2\ell}\right]$$
$$r_{\rm min} < r_{ij} < r_{\rm co}, \tag{4}$$

$$\phi_{\rm LJ}^{ij} = 0, \quad r_{ij} \geqslant r_{\rm co}. \tag{5}$$

Here $r_{\rm min}/\lambda$ is the length where the potential attains its minimum, and $r_{\rm co}/\lambda$ is the cutoff length for which the potential vanishes. The coefficients a, b, and $c_{2\ell}$ are chosen such that the repulsive and attractive parts of the potential are continuous with two derivatives at the potential minimum and the potential goes to zero continuously at $r_{\rm co}/\lambda$ with two continuous derivatives as well. The unit of length $\lambda = 1.0$ is set to be the interaction length scale of two particles, ε is the unit of energy, and the Boltzmann constant $k_B = 1$.

For any two successive particles within the k'th chain there is the finite nonelastic elongation (FENE) potential with finite length r_0, which is defined as

$$\chi_k^{i,i+1}(r) = \begin{cases} -\frac{1}{2}\eta r_0^2 \ln[1-(r/r_0)^2]; & r < r_0 \\ \infty; & r \geqslant r_0 \end{cases}, \tag{6}$$

where $r \equiv r_{i,i+1}/\lambda$ and η is a parameter with units of force per unit length.

Finally, for any three successive monomers within the k'th oligomer with vertex i there is an angle constraint around a chosen equilibrium angle $\varphi^{\rm eq}$ and is defined as

$$\psi_k^{i-1,i,i+1}(\varphi^i) = \kappa\left[\cos\varphi_k^i - \cos\varphi^{\rm eq}\right]^{\alpha} = \kappa\left[1+\cos\varphi_k^i\right]^{\alpha}. \tag{7}$$

Below we will also employ the angle θ where $\theta \equiv \pi - \varphi$. Thus for a stiff polymer $\varphi \approx \pi$ while θ is close to zero.

We distinguish between two cases, that of a stiff oligomer with $\alpha = 1$ and a semiflexible oligomer with $\alpha = 2$. The meaning of the words "stiff" and "semiflexible" will be made clear in the sequel. The values of all the parameters used in the simulation are given in Table I.

III. NUMERICAL SIMULATIONS

We prepare a two-dimensional system consisting of 256 polymers having 20 monomers in a chain. The initial density $\rho = 0.8$, and the temperature is chosen such that the system is in the liquid state with high temperature $T = 1.3$. To achieve such a state we begin with the crystalline arrangement of the polymers on a square lattice, and we allow the crystal to melt by molecular dynamics. The masses of the monomers are all unity. The melt is equilibrated using a standard *NPT* procedure for 25 τ_α LJ time units at pressure $P = 1.0$ (LJ units), where τ_α is the alpha relaxation time. This relaxation time is measured using the intermediate scattering function in the usual manner [8]. In Fig. 1 we present the scattering function as a function of time and the resulting relaxation time for various temperatures, for $\kappa = 0$ and $\kappa = 2$. Defining (arbitrarily) the glass transition temperature T_g as the temperature where the Arrhenius behavior changes to faster $1/T$ dependence, we observe that T_g increases from $T_g \approx 0.5$ to $T_g \approx 0.6$ as κ increases from $\kappa = 0$ to $\kappa = 2$. We expect this trend to continue [8].

After equilibration the polymer melt is coupled to a heat bath at temperature $T = 0.01$ (LJ units) and constant pressure ($P = 1$). The system is then further equilibrated for another 100 LJ time units. Finally the glass sample is taken to the nearest inherent minimum state using a conjugate gradient scheme. This protocol is referred to as "infinitely fast" quench.

Having prepared the oligomeric glass sample it is subjected to an athermal quasistatic strain (AQS) as described in detail in Ref. [11]. In brief, each monomer is first displaced by the affine transformation

$$x_i \to x_i + \delta\gamma\, y_i, \quad y_i \to y_i, \tag{8}$$

where $r_i \equiv (x_i, y_i)$ is the initial position of the ith monomer and $\delta\gamma$ is the strain step applied during each affine transformation. The above transformation leads to nonzero resultant forces on the monomers. These forces are annulled by a nonaffine transformation $r_i \to r_i + u_i$, where u_i is displacement of the monomer necessary to return to mechanical equilibrium. The nonaffine displacement is computed using the conjugate gradient scheme. The strain step is chosen for the present study is $\delta\gamma = 10^{-4}$. The simulation is performed under periodic boundary conditions along each direction of the box using the Lees-Edward formalism. In all the discussion bellow, including the figures, the value of the strain γ will be computed as a sum over the steps $\delta\gamma$ appearing in Eq. (8).

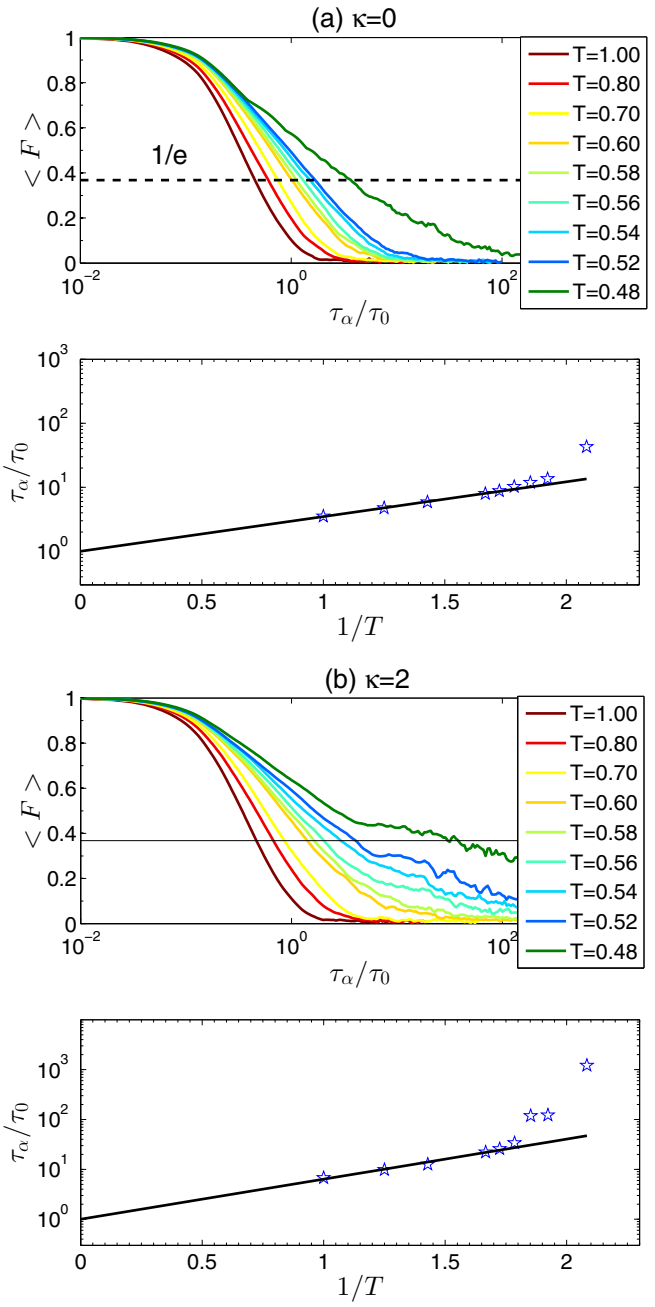

FIG. 1. (Color online) The intermediate scattering function vs time (for various temperatures) and the relaxation time vs inverse temperature. Upper panel: $\kappa = 0$; lower panel: $\kappa = 2$.

We consider both stiff and semiflexible polymers in our studies [see Eq. (7)]. For stiff polymers the results will be presented for $\kappa = 2,5,10$, and 15; for the semiflexible case we consider $\kappa = 2,4,8$, and 10. Unless stated specifically the results reported below will refer to the stiff oligomer case with $\alpha = 1$.

A. Mechanical response of the polymer

A typical stress versus strain curve that results in the AQS protocol is shown in Fig. 2 for a single realization of a stiff oligomeric glass with $\kappa = 2$. The stress grows linearly at first

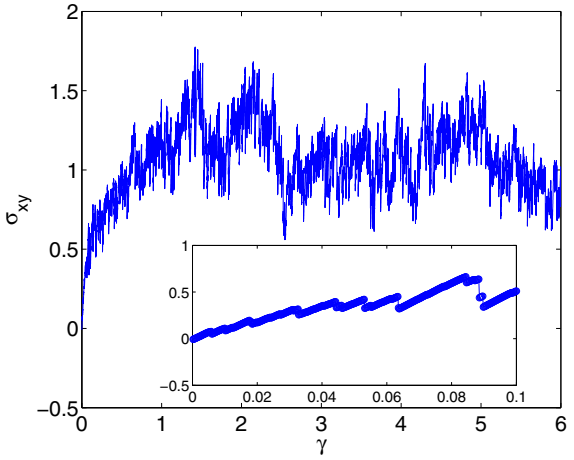

FIG. 2. (Color online) A typical stress vs strain curve obtained by AQS straining of 256 polymers of chain length 20 with stiffness parameter $\kappa = 2$. Smooth (linear) increases in the strain are punctuated with sharp drops. The trajectory of stress vs strain is reversible only until the first drop. The sharp drops are plastic events as explained in the text. Inset: Blow-up of the first few plastic drops.

with the strain, and the protocol can be reversed to return to initial state. Upon increasing the strain the stress versus strain trajectory gets punctuated with sharp drops; these are irreversible, and after the occurrence of the first one we cannot return to the initial state by reversing the protocol. After each plastic drop the stress rises again linearly with the applied strain (but not necessarily with the same slope) until the next plastic drop takes place. Generally speaking both the stress versus strain and the energy versus strain curves reach eventually a kind of steady state in which the average stress and energy do no longer change even though they still experience elastic increases and plastic drops. This type of response has been often described in the context of atomistic glasses; see, for example, Refs. [3,9–11]

At first, when the external strain is still small, the energy drops associated with the plastic events are small and do not increase with the system size. These plastic energy drops are associated with localized events as is explained in the next section. On the other hand, when the external strain is increased, at a threshold value of the external strain (also known as the yield strain γ_Y) much bigger energy drops become possible. Once the yield stress has been achieved, there is a quantitative change in the nature of the plastic drops since they become system-size dependent. We can examine the statistics of the magnitude of the energy and stress drops in the steady state. In Fig. 3 we show the average magnitude of energy $\langle \Delta U \rangle$ and stress drops $\langle \Delta \sigma \rangle$ for systems of increasing number of particles N. It appears that the data support the scaling laws

$$\langle \Delta U \rangle \sim N^{\tilde{\alpha}}, \quad \tilde{\alpha} \approx 0.5, \tag{9}$$

$$\langle \Delta \sigma \rangle \sim N^{\tilde{\beta}}, \quad \tilde{\beta} \approx -0.5. \tag{10}$$

In Ref. [11] it was shown that these exponents satisfy a scaling relation $\tilde{\alpha} - \tilde{\beta} = 1$ as these exponents do. Since the system spanning events are confined to linear structures one is not surprised with the exponent $\tilde{\alpha} = 1/2$ in a two-dimensional

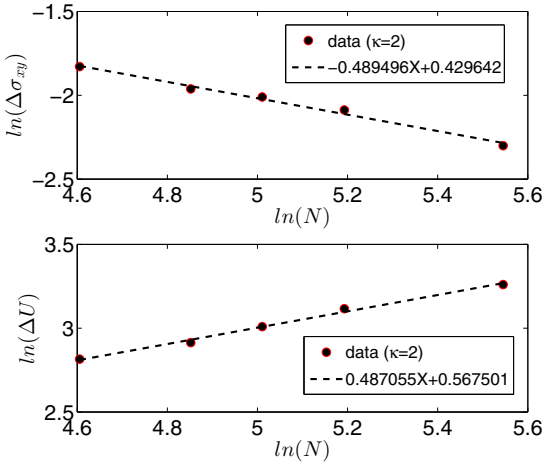

FIG. 3. (Color online) Log-log plots of the average magnitude of the stress drops $\Delta\sigma$ and energy drops ΔU in the steady state (after the yield strain had been passed) as a function of the number of particles in the system.

system. The scaling relation immediately determines also $\tilde{\beta} = -1/2$.

To make sure that the exponent $\tilde{\alpha} = 0.5$ is consistent we can test the probability distribution functions (pdf) of the energy or stress drops. In Fig. 4 we show the raw pdfs of these quantities and the rescaled pdf's. The rescaling is done using the exponent $\tilde{\alpha} = 1/2$. The data collapse of the pdfs in the tails shows that the exponent is adequate. Note that the rescaling does not collapse the data for small drops; these continue to be system size independent.

A theoretical discussion of the localized and the subextensive plastic events is provided in Sec. IV. Nevertheless the reader should note that a continuum description of the stress versus strain curves in our amorphous solids is still under debate, even in the case of simpler examples like binary Lennard-Jones glasses. Here the quantitative theory of energy input by mechanical strain, including the share taken by stress versus oligomeric conformation changes on the one hand, and energy dissipated to the heat bath on the other hand is

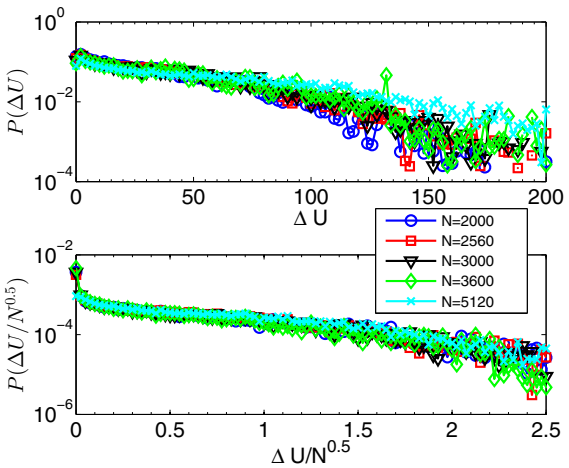

FIG. 4. (Color online) Raw and rescaled pdf's for the energy drops in the steady state. The data collapse in the tails of the distributions supports the scaling laws presented in Eqs. (9) and (10).

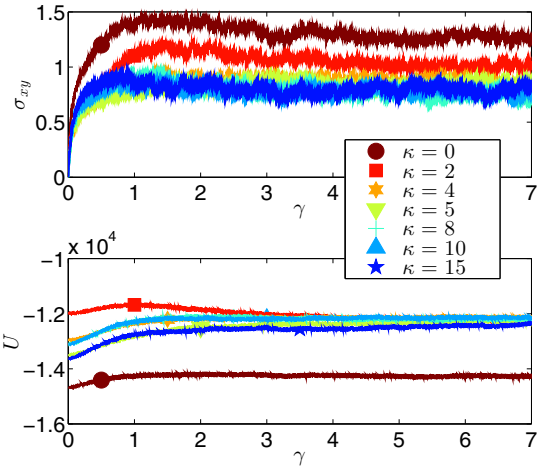

FIG. 5. (Color online) Upper panel: Stress vs strain for different κ for the stiff polymer ($\alpha = 1$). The stress reaches to the same steady state for the finite κ. Bottom panel: The variation of total internal potential energy with strain. The data averaged over 40 independent realizations are shown.

still unavailable. Such an understanding is prerequisite to any continuum theory.

B. Stress and energy averaged over realizations as a function of the stiffness parameter

In addition to measuring the plastic drops in a single realization of the glass, it is interesting to examine the energy and the stress averaged over many realizations. Such graphs should be closer to what is expected in the thermodynamic limit when $N_p \to \infty$. In particular we can examine the dependence on the stiffness parameter κ. In Fig. 5 we see the stress versus strain and the energy versus strain averaged over 40 independent realizations as a function of κ. It is interesting to see that both the energy reaches the same steady state for $\kappa \neq 0$, but not for $\kappa = 0$. The stress appears to reach the same steady state for $\kappa > 2$, but not for $\kappa = 0,2$. To underline the fact that the attainment of the same steady state energy is not at all trivial, we show in Fig. 6 the dependence on the strain of the various contributions to the energy coming from the different terms in the Hamiltonian. It is quite evident that the various contributions to the total energy do *not* reach the same steady state, and the result shown in Fig. 5 is the consequence of an interesting and subtle cancellation that needs to be explained. Currently we have no explanation to this observation. To be more confident in the correctness of the observation we changed the parameter η in Eq. (6) and repeated the measurements; the observation remains invariant.

C. Changes in geometry of polymers with applied strain

In addition to the energy and the stress in the system, the oligomeric glass presents also interesting responses to external strains in the resulting geometry of the chains. Of course, the configuration of the oligomers in the glass depends on the stiffness of the chains. In order to characterize the configuration of the oligomer chains we compute the end-to-end

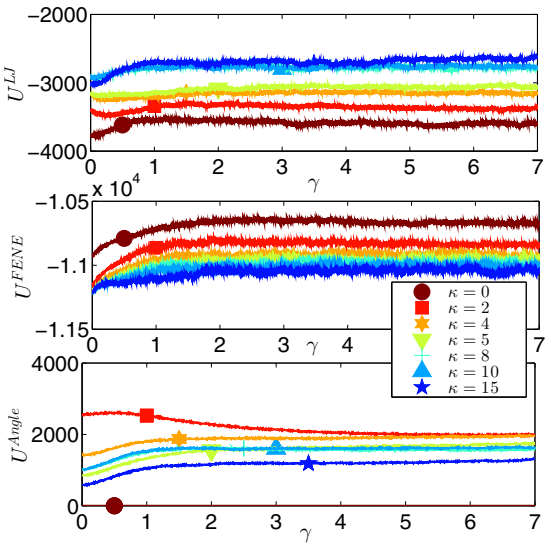

FIG. 6. (Color online) Variation of the three individual contributions to the total potential energy arising from different interactions of each with strain. Upper panel: $U_{\rm LJ}$ vs strain for different κ. The potential energy due to the LJ interaction increases on increase of κ. Middle panel: $U_{\rm FENE}$ vs strain for different κ. Bottom panel: $U_{\rm angle}$ vs strain. The potential energy $U_{\rm angle}$ decreases on increase of the stiffness of the chain.

length R_{ee} of the chain and follow how it changes with the applied strain. Figure 7 shows the variation of R_{ee} for the stiff case as the applied strain is increased. We see that the tendency is different for small and large value of κ. For small κ the chains start from a coiled state, with R_{ee} being of the order of $\sqrt{n}$. Then the action of the strain tends to straighten the chains to increase R_{ee} until a κ-dependent steady state. On the other hand, for large κ one starts with almost straight chains, such that the R_{ee} is of the order of n; straining now leads to bending, increasing the energy of the system, reaching again a κ-dependent steady state. The process described can be seen directly in snapshots of the system under strain. This is shown for $\kappa = 0$ and $\kappa = 10$ in Fig. 8.

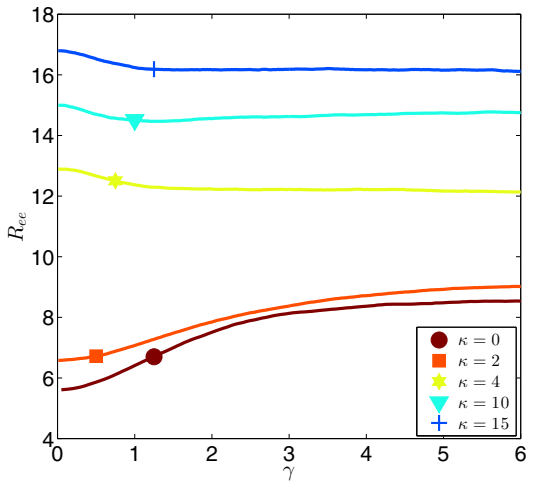

FIG. 7. (Color online) Variation of end to end length R_{ee} of the stiff polymers with the applied strain γ as a function of κ.

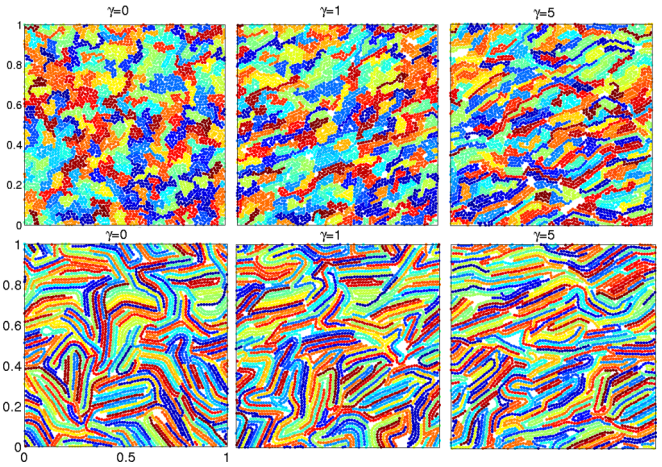

FIG. 8. (Color online) Snapshot of the polymer in the box for $\kappa = 0$ (upper panel) and $\kappa = 10$ (lower panel). From left to right: (a) $\gamma = 0$, (b) $\gamma = 1$, and (c) $\gamma = 5$. For $\kappa = 0$ the polymers are coiled for zero strain, and they stretch on average upon increasing of the strain. The opposite occurs for $\kappa = 10$.

D. Theoretical remarks on the end-to-end distance and the average angular distribution

The first observation that needs to be explained is the end-to-end distance in equilibrium (at $\gamma = 0$). It turns out that just using the angular potential is sufficient to give a good estimate of this distance. The reason is that because the oligomers are fairly stiff, the Lennard Jones term does not lead to strong short-range particle-particle repulsion, while the main effect of the FENE term is simply to renormalize the individual interbond distances. Thus using the angular potential we can simply calculate the average angle of the oligomer chain which given by

$$\langle \cos\theta \rangle = \frac{\int_0^\pi d\theta \cos\theta \exp\left(-\frac{U_{\rm Angle}}{T}\right)}{\int_0^\pi d\theta \exp\left(-\frac{U_{\rm Angle}}{T}\right)}. \tag{11}$$

Here the temperature T should be taken to be of the order of the fluid melt from which the glass was quenched. Below we take $T = 1$. This integral can be performed exactly, and its value is $I_1(\kappa/T)/I_0(\kappa/T)$ where I_1 and I_0 are the modified Bessel function of order 1 and 0, respectively. In the upper panel of Fig. 9 we compare the theoretical evaluation of $\langle \cos\theta \rangle$ to its numerically computed counterpart and conclude the comparison is good.

Using the average angle we can write the average value $\langle R_{ee} \rangle$ [19] as

$$\left\langle R_{ee}^2 \right\rangle = n\left[\frac{1+\langle\cos\theta\rangle}{1-\langle\cos\theta\rangle} - \frac{1}{n}\frac{2\langle\cos\theta\rangle(1-\langle\cos\theta\rangle^n)}{(1-\langle\cos\theta\rangle)^2}\right]. \tag{12}$$

Taking the square root of this expression we plot it in the middle panel of Fig. 9 and compare it with the numerically calculated value of R_{ee} at $\gamma = 0$, averaged over 40 different initial conditions. The agreement is quite acceptable.

Finally, it is advantageous to define "persistence length" ℓ_p using the relationship

$$\langle \cos\theta \rangle \equiv \exp(-1/\ell_p). \tag{13}$$

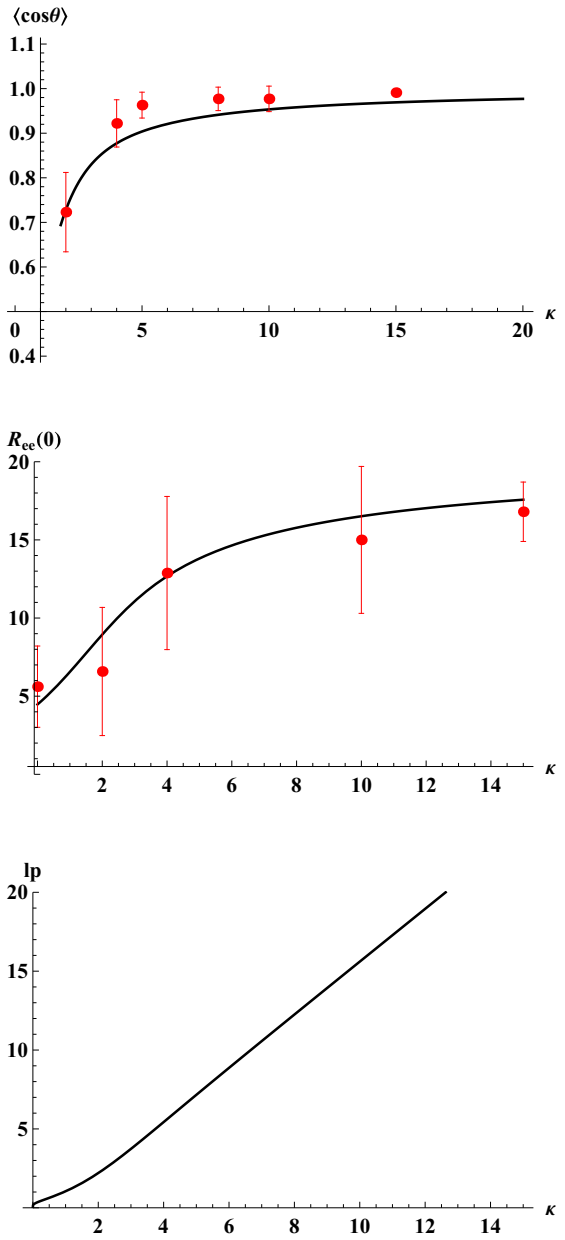

FIG. 9. (Color online) The average angular measure $\langle \cos\theta \rangle$ (upper panel), the average equilibrium end-to-end length $R_{ee}(0)$ (middle panel,) and the average persistence length (ℓ_p) (lower panel) as a function of κ at zero strain ($\gamma = 0$). The red dots with error bars are the data obtained from numerical simulations, and black curves are the theoretical estimates obtained using the theory discussed in Sec. III D.

The resulting ℓ_p for $\gamma = 0$ is shown in the lower panel of Fig. 9. We note that the persistence length becomes of the order of R_{ee} when the latter is about 10.

Returning to Fig. 7 one notes three interesting features:

(1) For small values of κ the end-to-end distance rises with increasing strain.

(2) For large values of κ the end-to-end distance decreases with increasing strain.

(3) In either case the end-to-end distance attains a κ-dependent asymptotic value for large γ, which is nevertheless *not* the fully stretched state.

For κ small there is a simple estimate of the asymptotic value of R_{ee} which involves a balance between the force due to straining, which tends to stretch the oligomer, and the entropic force, which tends to keep the oligomer coiled. Estimating the force due to stress as σR and the entropic force as $\frac{T}{R_{ee}^2}(R - R_{ee})$ [20]. Balancing the two expressions we predict that

$$R_{ee}(\sigma) = \frac{R_{ee}(\sigma = 0)}{1 - \sigma R_{ee}^2(\sigma = 0)/T}. \tag{14}$$

Indeed, the observed increase in the end-to-end distance at small values of κ is in accordance with this prediction. Of course for larger values of σ the FENE terms need to be invoked to cure the apparent divergence in Eq. (14). Note that this argument pertains only for small κ. At larger values of this parameter the angular contribution can dominate over the pure entropic contribution.

Once the persistence length is of the order of the initial value of R_{ee} we can assume that the oligomers are entirely stretched. Then the effect of the shear strain is opposite, in reducing the end-to-end distance. This stems simply from the fact that any inclined stretched polymer will bend under the action of shear, since its two ends move at different speeds. The reader can see this phenomenon occurring in the lower panel of Fig. 8. Thus the effect of increasing γ will initially decrease R_{ee} as is observed in Fig. 7.

In both cases the estimate of the asymptotic value of R_{ee} is not easy, and we leave it for future research.

IV. THEORY OF PLASTIC EVENTS

The stability of amorphous solids is determined by the Hessian matrix which is made of second derivatives of the Hamiltonian with respect to all the degrees of freedom. This matrix is always symmetric and real and therefore diagonalizable. As long as all the eigenvalues are positive, the system is mechanically stable. Plastic instabilities are characterized by an eigenvalue going to zero signaling the loss of mechanical stability.

A. Calculation of the Hessian matrix

To calculate the Hessian matrix for the oligomeric glass we recognize the three contributions to the potential energy $\phi_{\rm LJ}$, χ, and ψ. These contributions result in three sub matrices that need to be summed up to yield the full Hessian. We denote the submatrices as $\mathcal{H}^{\rm LJ}$, $\mathcal{H}^{\rm FENE}$, and $\mathcal{H}^{\rm Angle}$:

$$\mathcal{H} = \mathcal{H}^{\rm LJ} + \mathcal{H}^{\rm FENE} + \mathcal{H}^{\rm Angle}. \tag{15}$$

We begin with $H^{\rm LJ}$:

$$\mathcal{H}^{\rm LJ}(i,j;\alpha,\beta) = \frac{\partial^2 \phi_{\rm LJ}^{ij}}{\partial x_\beta^j \partial x_\alpha^i} = \frac{\partial^2 \phi_{\rm LJ}^{ij}}{\partial (r^{ij})^2} \frac{\partial r^{ij}}{\partial x_\beta^j} \frac{\partial r^{ij}}{\partial x_\alpha^i} + \frac{\partial \phi_{\rm LJ}^{ij}}{\partial r^{ij}} \frac{\partial^2 r^{ij}}{\partial x_\beta^j \partial x_\alpha^i}, \tag{16}$$

and for $i = j$ it is

$$\mathcal{H}^{\mathrm{LJ}}(i,i;\alpha,\beta) = \sum_{\mathrm{j}\neq\mathrm{i}} -\mathcal{H}^{\mathrm{LJ}}(i,j;\alpha,\beta). \tag{17}$$

Note that unless otherwise stated Latin letters (e.g., i, j, etc.) will be used for the particle's coordinate, and Greek letters (e.g., α,β, etc.) will be used to the denote the displacement coordinate of the particles. In order to compute the terms used in the above equation [Eq. (16)] explicitly, we take the advantage of the identities:

$$\frac{\partial r^{m\ell}}{\partial x^i_\alpha} = \frac{r^{m\ell}_\alpha}{r^{m\ell}}(\delta^{\ell i} - \delta^{mi}) \tag{18}$$

and

$$\frac{\partial^2 r^{m\ell}}{\partial x^j_\beta \partial x^i_\alpha} = \left[\frac{\delta_{\alpha\beta}}{r^{m\ell}} - \frac{r^{m\ell}_\alpha r^{m\ell}_\beta}{(r^{m\ell})^3}\right]\left(\delta^{\ell j} - \delta^{mj}\right)\left(\delta^{\ell i} - \delta^{mi}\right). \tag{19}$$

Now we consider the terms in which the bond of a polymer connecting particles k and ℓ contributes to the $\mathcal{H}^{\mathrm{FENE}}$. These terms are written as

$$\mathcal{H}^{\mathrm{FENE}}(k,l;\alpha,\beta) = \begin{pmatrix} \frac{\partial^2\chi^{k\ell}}{\partial x^k_\alpha \partial x^k_\beta} & \frac{\partial^2\chi^{k\ell}}{\partial x^k_\alpha \partial x^\ell_\beta} \\ \frac{\partial^2\chi^{k\ell}}{\partial x^\ell_\alpha \partial x^k_\beta} & \frac{\partial^2\chi^{k\ell}}{\partial x^\ell_\alpha \partial x^\ell_\beta} \end{pmatrix}, \tag{20}$$

where α and β stand for all coordinates, and thus the dimensions of A are $2d \times 2d$. The four entries of matrix A are not necessarily adjacent in $\mathcal{H}^{\mathrm{FENE}}$; depending on the values of k and ℓ they are positioned at (dk,dk), $(dk,d\ell)$, $(d\ell,dk)$, and $(d\ell,d\ell)$, respectively, where d is the dimensionality of the system.

Further we consider the terms related to the ith valence angle within a polymer chain. This angle is defined by three successive particles with indices k, ℓ, and m. The contribution of these terms to the Hessian $\mathcal{H}^{\mathrm{Angle}}$ is expressed as

$$\mathcal{H}^{\mathrm{Angle}} = \begin{pmatrix} \frac{\partial^2\psi^i}{\partial x^k_\alpha \partial x^k_\beta} & \frac{\partial^2\psi^i}{\partial x^k_\alpha \partial x^\ell_\beta} & \frac{\partial^2\psi^i}{\partial x^k_\alpha \partial x^m_\beta} \\ \frac{\partial^2\psi^i}{\partial x^\ell_\alpha \partial x^k_\beta} & \frac{\partial^2\psi^i}{\partial x^\ell_\alpha \partial x^\ell_\beta} & \frac{\partial^2\psi^i}{\partial x^\ell_\alpha \partial x^m_\beta} \\ \frac{\partial^2\psi^i}{\partial x^m_\alpha \partial x^k_\beta} & \frac{\partial^2\psi^i}{\partial x^m_\alpha \partial x^\ell_\beta} & \frac{\partial^2\psi^i}{\partial x^m_\alpha \partial x^m_\beta} \end{pmatrix}, \tag{21}$$

where α and β stand for all coordinates, and thus the dimensions of $\mathcal{H}_{\mathrm{Angle}}$ are $3d \times 3d$. The four entries of $\mathcal{H}_{\mathrm{Angle}}$ are not necessarily adjacent; depending on the values of k, ℓ, and m they are positioned at (dk,dk), $(dk,d\ell)$, (dk,dm), $(d\ell,dk)$, $(d\ell,d\ell)$, $(d\ell,dm)$, (dm,dk), $(dm,d\ell)$, and (dm,dm), respectively, where d is dimensionality of the system.

Formally the angular contribution to the Hessian can be expressed as

$$\begin{aligned}\mathcal{H}_{\mathrm{Angle}}(i,j;\alpha,\beta) &= \frac{\partial^2\psi^\ell}{\partial x^j_\beta \partial x^i_\alpha} \\ &= \frac{\partial^2\psi^\ell}{(\partial\cos\varphi^\ell)^2}\frac{\partial\cos\varphi^\ell}{\partial x^i_\alpha}\frac{\partial\cos\varphi^\ell}{\partial x^j_\beta} \\ &\quad + \frac{\partial\psi^\ell}{\partial\cos\varphi^\ell}\frac{\partial^2\cos\varphi^\ell}{\partial x^j_\beta \partial x^i_\alpha},\end{aligned} \tag{22}$$

where the cosine of the valence angle is defined as

$$\cos\varphi^l = -\frac{r^{l-1,l}_\gamma r^{l,l+1}_\gamma}{r^{l-1,l} r^{l,l+1}},$$

with $r^{kl}_\gamma = r^l_\gamma - r^k_\gamma$. Now inserting the formula for cosine in Eq. (22), one obtains

$$\begin{aligned}\frac{\partial\cos\varphi^l}{\partial x^m_\alpha} &= -\left[\frac{r^{l,l+1}_\gamma}{r^{l,l+1}}\frac{\partial}{\partial x^m_\alpha}\left(\frac{r^{l-1,l}_\gamma}{r^{l-1,l}}\right) + \frac{r^{l-1,l}_\gamma}{r^{l-1,l}}\frac{\partial}{\partial x^m_\alpha}\left(\frac{r^{l,l+1}_\gamma}{r^{l,l+1}}\right)\right], \\ \frac{\partial^2\cos\varphi^l}{\partial x^m_\alpha \partial x^q_\beta} &= -\left[\frac{r^{l,l+1}_\gamma}{r^{l,l+1}}\frac{\partial^2}{\partial x^m_\alpha \partial x^q_\beta}\left(\frac{r^{l-1,l}_\gamma}{r^{l-1,l}}\right) + \frac{r^{l-1,l}_\gamma}{r^{l-1,l}}\frac{\partial^2}{\partial x^m_\alpha \partial x^q_\beta}\left(\frac{r^{l,l+1}_\gamma}{r^{l,l+1}}\right)\right. \\ &\quad \left. + \frac{\partial}{\partial x^m_\alpha}\left(\frac{r^{l-1,l}_\gamma}{r^{l-1,l}}\right)\frac{\partial}{\partial x^q_\beta}\left(\frac{r^{l,l+1}_\gamma}{r^{l,l+1}}\right) + \frac{\partial}{\partial x^q_\beta}\left(\frac{r^{l-1,l}_\gamma}{r^{l-1,l}}\right)\frac{\partial}{\partial x^m_\alpha}\left(\frac{r^{l,l+1}_\gamma}{r^{l,l+1}}\right)\right].\end{aligned}$$

The other auxiliary expressions are given by

$$\begin{aligned}\frac{\partial}{\partial x^m_\alpha}\left(\frac{r^{kl}_\gamma}{r^{kl}}\right) &= \left(\frac{\delta_{\alpha\gamma}}{r^{kl}} - \frac{r^{kl}_\alpha r^{kl}_\gamma}{(r^{kl})^3}\right)(\delta^{lm} - \delta^{km}), \\ \frac{\partial^2}{\partial x^m_\alpha \partial x^q_\beta}\left(\frac{r^{kl}_\gamma}{r^{kl}}\right) &= \left[\frac{3r^{kl}_\alpha r^{kl}_\beta r^{kl}_\gamma}{(r^{kl})^5} - \frac{\delta_{\alpha\beta}r^{kl}_\gamma + \delta_{\alpha\gamma}r^{kl}_\beta + \delta_{\beta\gamma}r^{kl}_\alpha}{(r^{kl})^3}\right](\delta^{lm} - \delta^{km})(\delta^{lq} - \delta^{kq}).\end{aligned}$$

.

Combining the above expressions we have

$$\begin{aligned}\frac{\partial\cos\varphi^l}{\partial x^m_\alpha} &= -\left[\frac{r^{l,l+1}_\gamma}{r^{l,l+1}}\frac{\partial}{\partial x^m_\alpha}\left(\frac{r^{l-1,l}_\gamma}{r^{l-1,l}}\right) + \frac{r^{l-1,l}_\gamma}{r^{l-1,l}}\frac{\partial}{\partial x^m_\alpha}\left(\frac{r^{l,l+1}_\gamma}{r^{l,l+1}}\right)\right] \\ &= -\left\{(\delta^{l,m} - \delta^{l-1,m})\left[\frac{r^{l,l+1}_\alpha}{r^{l,l+1}r^{l-1,l}} - \frac{r^{l-1,l}_\alpha r^{l-1,l}_\gamma r^{l,l+1}_\gamma}{r^{l,l+1}(r^{l-1,l})^3}\right] + (\delta^{l+1,m} - \delta^{l,m})\left[\frac{r^{l-1,l}_\alpha}{r^{l,l+1}r^{l-1,l}} - \frac{r^{l,l+1}_\alpha r^{l-1,l}_\gamma r^{l,l+1}_\gamma}{r^{l-1,l}(r^{l,l+1})^3}\right]\right\},\end{aligned}$$

$$\frac{\partial^2 \cos\varphi^l}{\partial x_\alpha^m \partial x_\beta^q} = -\Bigg[\frac{r_\gamma^{l,l+1}}{r^{l,l+1}}\frac{\partial^2}{\partial x_\alpha^m \partial x_\beta^q}\left(\frac{r_\gamma^{l-1,l}}{r^{l-1,l}}\right) + \frac{r_\gamma^{l-1,l}}{r^{l-1,l}}\frac{\partial^2}{\partial x_\alpha^m \partial x_\beta^q}\left(\frac{r_\gamma^{l,l+1}}{r^{l,l+1}}\right)$$
$$+ \frac{\partial}{\partial x_\alpha^m}\left(\frac{r_\gamma^{l-1,l}}{r^{l-1,l}}\right)\frac{\partial}{\partial x_\beta^q}\left(\frac{r_\gamma^{l,l+1}}{r^{l,l+1}}\right) + \frac{\partial}{\partial x_\beta^q}\left(\frac{r_\gamma^{l-1,l}}{r^{l-1,l}}\right)\frac{\partial}{\partial x_\alpha^m}\left(\frac{r_\gamma^{l,l+1}}{r^{l,l+1}}\right)\Bigg]$$
$$= -\Bigg\{\left[\frac{3r_\alpha^{l-1,l}r_\beta^{l-1,1}r_\gamma^{l-1,l}r_\gamma^{l,l+1}}{r^{l,l+1}(r^{l-1,l})^5} - \frac{\left(\delta_{\alpha\beta}r_\gamma^{l-1,l}r_\gamma^{l,l+1} + r_\alpha^{l,l+1}r_\beta^{l-1,1} + r_\alpha^{l-1,1}r_\beta^{l,l+1}\right)}{r^{l,l+1}(r^{l-1,l})^3}\right](\delta^{lm} - \delta^{l-1,m})(\delta^{lq} - \delta^{l-1,q})$$
$$+\left[\frac{3r_\alpha^{l,l+1}r_\beta^{l,1+1}r_\gamma^{l-1,l}r_\gamma^{l,l+1}}{r^{l-1,l}(r^{l,l+1})^5} - \frac{\left(\delta_{\alpha\beta}r_\gamma^{l-1,l}r_\gamma^{l,l+1} + r_\alpha^{l,l+1}r_\beta^{l-1,1} + r_\alpha^{l-1,1}r_\beta^{l,l+1}\right)}{r^{l-1,l}(r^{l,l+1})^3}\right](\delta^{l+1,m} - \delta^{l,m})(\delta^{l+1,q} - \delta^{l,q})$$
$$+\left[\frac{\delta_{\alpha\beta}}{r^{l-1,l}r^{l,l+1}} - \frac{r_\alpha^{l-1,l}r_\beta^{l-1,1}}{r^{l,l+1}(r^{l-1,l})^3} - \frac{r_\alpha^{l,l+1}r_\beta^{l,1+1}}{r^{l-1,l}(r^{l,l+1})^3} + \frac{r_\alpha^{l-1,l}r_\beta^{l,1+1}r_\gamma^{l-1,l}r_\gamma^{l,l+1}}{(r^{l-1,l})^3(r^{l,l+1})^3}\right](\delta^{l,m} - \delta^{l-1,m}](\delta^{l+1,q} - \delta^{l,q})$$
$$+\left[\frac{\delta_{\alpha\beta}}{r^{l-1,l}r^{l,l+1}} - \frac{r_\alpha^{l-1,l}r_\beta^{l-1,1}}{r^{l,l+1}(r^{l-1,l})^3} - \frac{r_\alpha^{l,l+1}r_\beta^{l,1+1}}{r^{l-1,l}(r^{l,l+1})^3} + \frac{r_\alpha^{l,l+1}r_\beta^{l-1,1}r_\gamma^{l-1,l}r_\gamma^{l,l+1}}{(r^{l-1,l})^3(r^{l,l+1})^3}\right](\delta^{l+1,m} - \delta^{l,m}](\delta^{l,q} - \delta^{l-1,q})\Bigg\}.$$

B. Elementary plastic events

Having calculated the Hessian matrix we can now examine the elementary plastic events that occur at small values of γ. As said above, the mechanical stability is lost when an eigenvalue of the Hessian goes to zero. This is occurring via a saddle-node bifurcation in which the minimum in which the system resides collides with a saddle of the global energy surface. During a saddle node bifurcation the approach of the eigenvalue to zero is generic, following a square-root singularity [11]

$$\lambda_p \sim \sqrt{\gamma_p - \gamma}, \tag{23}$$

where λ_P is the eigenvalue that reaches zero at $\gamma = \gamma_P$. An example of this square-root singularity for a stiff oligomeric glass with $\kappa = 2$ is shown in Fig. 10. As the instability is approached the nonaffine response becomes closer to the eigenvector of the Hessian matrix that is associated with λ_P, denoted as Ψ_P. This phenomenon is demonstrated in Fig. 11.

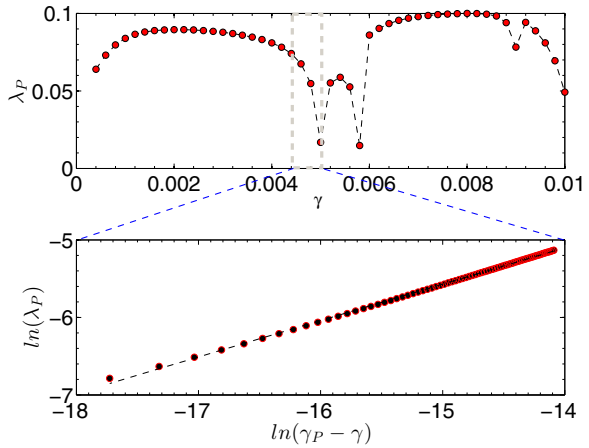

FIG. 10. (Color online) The variation of the smallest eigenvalue λ_P as γ is increased, In the upper panel we see the eigenvalue dips to zero, then recovers after the instability is over, and again dips to zero at the next instability. In the lower panel we choose to blow up the region of the first instability to demonstrate the approach of the eigenvalue to zero with a square-root singularity [Eq. (23)].

It is important to stress that the square-root singularity is generic and characteristic to saddle-node bifurcations. It should be therefore independent of the system parameters and even the nature of the system. In our case we demonstrate this universality by changing from stiff to semiflexible and measuring the eigenvalue λ_P for two values of κ as shown in Fig. 12.

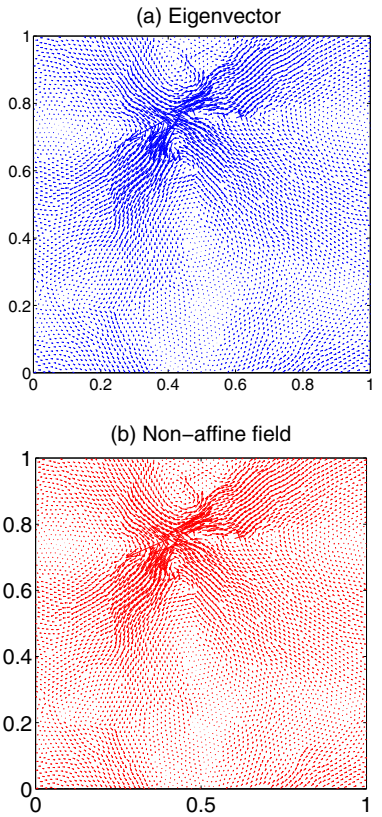

FIG. 11. (Color online) The eigenvector Ψ_P and the nonaffine displacement field associated with the first plastic instability as $\lambda \to 0$. The length units are normalized to the full length of the box.

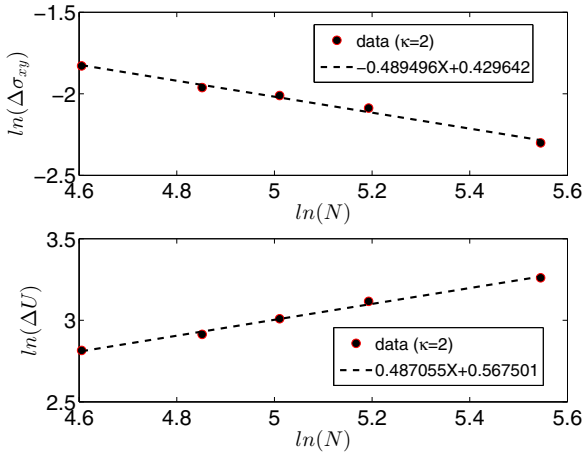

FIG. 12. (Color online) Log-log plot of the eigen value of the plastic mode λ_P vs $\gamma_P - \gamma$ for $\kappa = 2$ (top panel) and for κ=8 (bottom panel) near the first elementary plastic event for semiflexible ($\alpha = 2$) polymer. The exponent is approximately 0.5.

V. FORMATION OF SHEAR BANDS

Oligomeric glasses, like simple binary glasses and the much more complex metallic glasses, exhibit, in addition to localized plastic events also a second class of system spanning, shear localizing events. These events are precursors to shear banding, and they need a finite amount of stress or strain to accumulate before they become possible. In previous analysis it was shown that shear localizing events occur when the strain exceeds a value γ_Y which depends on the Poisson ratio of the material but is usually around 5%–7% [12]. It appears that the present oligomeric glasses are not much different in this respect. We begin to see shear localizing instabilities when γ is of the order of 10% or less. The shear localization event is rather dramatic; even though we shear homogeneously with our affine transformation the system chooses to respond by localizing all the shear over a small band of the size of the core of the Eshelby solution; see Refs. [12,13] for details. It was shown in Refs. [12,13] that this solution minimizes the energy compared to a random array of elementary plastic events.

The nature of the shear localizing events is similar to what had been seen previously: an eigenvalue of the Hessian matrix dips to zero, but now instead of a single quadrupolar structure a whole string of those, concatenated along a line in two dimensions [12] or on a plane in three dimensions [13], appear simultaneously. They have a global connection now, with the outgoing direction of one quadrupolar structure connecting immediately to the incoming direction of the next quadrupole, thus arranging the displacement field to go in two different direction above and below the line (or plane). For pure shear the line (or plane) is at 45° to the principal stress axis. Other angles are possible for uniaxial loading [21].

The best way to demonstrate the phenomenon is to display the eigenfunction or the displacement field associated with the event. In Fig. 13 we show both the eigenfunction in the upper panel and the directly simulated nonaffine displacement field at the instability in the lower panel. Both images show how the shear is now concentrated over a narrow band, with the displacement field pointing to the

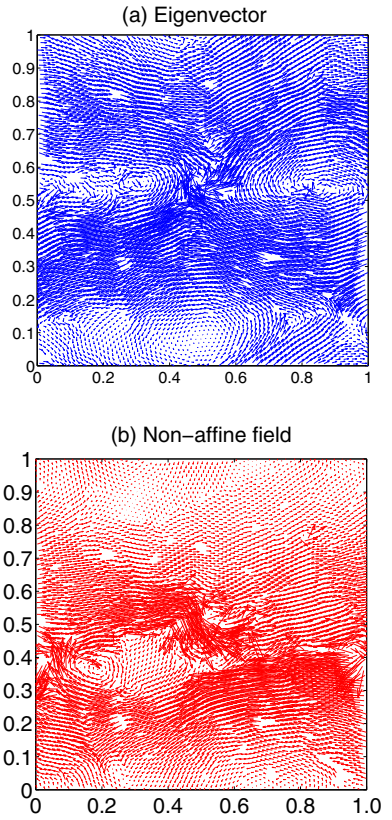

FIG. 13. (Color online) The eigenfunction Ψ_P and the nonaffine displacement field associated with a shear localizing plastic instability as $\lambda \to 0$. Note the global connection between the series of quadrupoles arranged along the line, such that the displacement field is pointing right above and left below the line. This IS the phenomenon of shear localization. The length units are normalized to the box size.

"right" above the band and to the "left" below the band. In a stress control rather than a strain controlled experiment such an event would lead to macroscopic failure.

In the next section we will present a theoretical formalism to compute the shear modulus for the oligomeric glasses.

VI. SHEAR MODULUS μ

The shear modulus that is a measure of linear elastic response of the material under the applied strain characterizes the mechanical behavior of the system. Here we provide the theory that relates the shear modulus to the microscopic variables like Hessian, nonaffine displacements, etc.

We recall that for homogeneous shear strain the shear modulus is defined as the second derivatives of the potential energy with respect to the applied strain γ, i.e.,

$$\mu = \frac{1}{V}\frac{d^2U(r_1, r_2, \ldots, r_N; \gamma)}{d\gamma^2}. \tag{24}$$

In this expression the second derivative contains two contributions: one coming from the affine part and another from the nonaffine motion of the monomers. Thus we have [22]

$$\frac{d}{d\gamma} = \frac{\partial}{\partial\gamma} + \frac{\partial}{\partial \mathbf{u_i}} \cdot \frac{\partial \mathbf{u_i}}{\partial\gamma} \equiv \frac{\partial}{\partial \mathbf{r_i}} \cdot \frac{\partial \mathbf{u_i}}{\partial\gamma}, \tag{25}$$

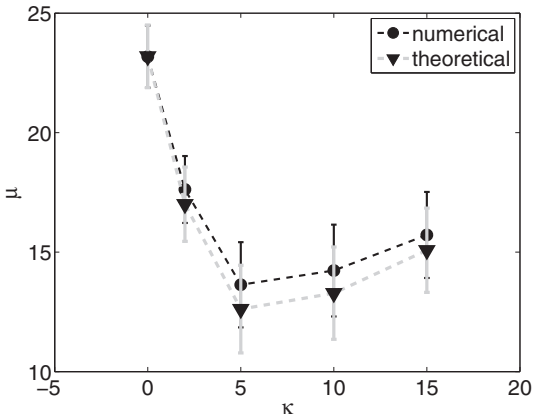

FIG. 14. Comparison of the theoretically calculated and the numerically estimated shear modulus for various values of κ. The relatively large error bars stem from the relative smallness of the system, in which different realizations give a spread of values of the shear modulus. Nevertheless the agreement between theory and simulations is quite satisfactory.

where the second equality follows from the relation $d\mathbf{r_i} = d\mathbf{u_i}$. Now the expression for shear modulus has the form

$$\mu = \frac{\partial^2 U}{\partial \gamma^2} + \frac{\partial u_i}{\partial \gamma}\frac{\partial U}{\partial r_i \partial \gamma}. \tag{26}$$

Further we note that the affine step is followed by the nonaffine step that returns the system to the equilibrium state. For the equilibrium state

$$\frac{df_i}{d\gamma} \equiv -\frac{d}{d\gamma}\frac{\partial U}{\partial r_i} = 0, \tag{27}$$

where f_i is the force on the ith particle. As we use the Eq. (25) in the above equation [Eq. (27)] we obtain

$$\frac{d\mathbf{u_i}}{d\gamma} = -H_{ij}^{-1} \cdot \Xi_j, \tag{28}$$

where H_{ij} is the Hessian and $\Xi_j = \frac{\partial^2 U}{\partial \gamma \partial r_j}$ is the nonaffine force. Now putting back Eq. (28) into Eq. (26) we obtain the expression for shear modulus as

$$\mu = \frac{1}{V}\frac{\partial^2 U(r_1, r_2, \ldots, r_n; \gamma)}{\partial \gamma^2} - \frac{1}{V}\sum_{i,j} \Xi_i \cdot H_{ij}^{-1} \cdot \Xi_j. \tag{29}$$

The first term in the above expression represents contribution in the shear modulus as a result of the affine displacement (also called as Born term), while the second one is the contribution due to the nonaffine responses. The Born term is computed analytically in Appendix A. The so-called "nonaffine force" $\boldsymbol{\Xi}$ is calculated directly from the knowledge of the potential (see the Appendix), and then we solve the inverted equation (28) $\boldsymbol{H} \cdot \frac{d\boldsymbol{u}}{d\gamma} = \boldsymbol{\Xi}$ using conjugate gradient minimization. Having at hand the nonaffine velocity $d\boldsymbol{u}/d\gamma$ we can get the nonaffine contribution to the shear modulus using Eq. (26).

A comparison between the theoretically calculated shear modulus and the one estimated directly from the stress versus strain curves at very small γ is provided in Fig. 14.

VII. SUMMARY AND CONCLUDING REMARKS

In this paper we discussed the mechanics of oligomeric glasses, also known as waxes, with a special attention to the stress and energy versus strain, the characteristics of the oligomeric chains and their changes under strain, the shear modulus, and the plastic failure modes. We proposed a microscopic outlook which extends the available theory for simple binary glasses to this much more complex oligomeric example. This resulted in an exact theory for the shear modulus, and a full understanding of the plastic failure, both in the localized and in the extended modes.

There are a few open problems that call for further theoretical and numerical considerations. The most relevant are the following:

(1) A continuum theory of the stress versus strain and energy versus strain is lacking. To be realistic, this is a hard task, and even for the simpler case of binary glasses such a theory is still under hard debate [23,24]. Understanding the energy budget will be crucial in achieving progress along these lines.

(2) A theory of the conformational changes of the oligomeric chain under strain was considered in Ref. [7], in particular the increase in the stress at large strains due to the global ordering. Here we have provided above a theory of the end-to-end distance for the case $\gamma = 0$ but not for finite γ.

(3) The extension of the approach to three dimensions is highly desirable. There one can expect interesting effects of oligomer interpenetration, trapping and reptation, especially with longer oligomers and under higher strains.

At least the last of these open issues is under active study in our laboratory, and we hope to present it in the near future.

APPENDIX: ANALYTIC COMPUTATION OF BORN TERMS

For small strain field the potential energy can be expressed as

$$U = U_0 + \frac{\partial U}{\partial \epsilon_{\alpha\beta}}\epsilon_{\alpha\beta} + \frac{1}{2}\frac{\partial^2 U}{\partial \epsilon_{\alpha\beta}\partial \epsilon_{\eta\nu}}\epsilon_{\alpha\beta}\epsilon_{\eta\nu} + O(\epsilon^3). \tag{A1}$$

Also for the simple shear with affine transformation h we have

$$h^T h = \begin{pmatrix} 1 & 0 \\ \gamma & 1 \end{pmatrix} \cdot \begin{pmatrix} 1 & \gamma \\ 0 & 1 \end{pmatrix} = \begin{pmatrix} 1 & \gamma \\ \gamma & 1+\gamma^2 \end{pmatrix} = 2\epsilon + I_2. \tag{A2}$$

Thus the strain field ϵ can be written as

$$\epsilon = \begin{pmatrix} 0 & \gamma/2 \\ \gamma/2 & \gamma^2/2 \end{pmatrix}. \tag{A3}$$

The Born contribution to the shear modulus μ_B can be expressed as

$$\mu_B \equiv \frac{d^2 U}{d\gamma^2} = \frac{\partial^2 U}{\partial \epsilon_{xy}^2} + \frac{\partial U}{\partial \epsilon_{yy}}. \tag{A4}$$

At this stage we need to compute the first and second derivative of the strained potential:

$$\frac{\partial U}{\partial \epsilon_{\alpha\beta}}; \quad \frac{\partial^2 U}{\partial \epsilon_{\alpha\beta}\partial \epsilon_{\eta\nu}}. \tag{A5}$$

Let us recall that for the polymer case the potential energy is given by

$$U = \sum_{\langle ij \rangle}^{N} \phi_{\mathrm{LJ}}^{ij} + \sum_{k=1}^{N_p}\sum_{i=1}^{n-1} \chi_k^i + \sum_{k=1}^{N_p}\sum_{i=2}^{n-1} \psi_k^i. \tag{A6}$$

Regarding the pairwise interactions we have

$$\frac{\partial U_{\mathrm{LJ\ or\ FENE}}}{\partial \epsilon_{\alpha\beta}} = \frac{\partial \phi_{\mathrm{LJ}}^{ij}}{\partial r^{ij}} \frac{\partial r^{ij}}{\partial \epsilon_{\alpha\beta}} \quad \text{or} \quad \frac{\partial \chi^{ij}}{\partial r^{ij}} \frac{\partial r^{ij}}{\partial \epsilon_{\alpha\beta}}. \tag{A7}$$

In order to compute $\partial r_{ij}/\partial \epsilon_{\alpha\beta}$ we define the change in r^{ij} using $\hat{r}_\alpha^{ij} = h_{\alpha\beta} r_\beta^{ij}$. Therefore,

$$\hat{r}^{ij} = \sqrt{\left(\hat{r}_\lambda^{ij}\right)^2} \tag{A8}$$

$$= \sqrt{r_\alpha^{ij} h^T h r_\beta^{ij}} \tag{A9}$$

$$\approx \sqrt{(r^{ij})^2 + 2\epsilon_{\alpha\beta} r_\alpha^{ij} r_\beta^{ij}} \tag{A10}$$

$$= r^{ij}\sqrt{1 + \frac{2\epsilon_{\alpha\beta} r_\alpha^{ij} r_\beta^{ij}}{(r^{ij})^2}} \tag{A11}$$

$$\approx r^{ij}\left[1 + \frac{\epsilon_{\alpha\beta} r_\alpha^{ij} r_\beta^{ij}}{(r^{ij})^2} - \frac{1}{2}\frac{\left(\epsilon_{\alpha\beta} r_\alpha^{ij} r_\beta^{ij}\right)^2}{(r^{ij})^4} + O(\epsilon^3)\right] \tag{A12}$$

$$= r^{ij} + \frac{\epsilon_{\alpha\beta} r_\alpha^{ij} r_\beta^{ij}}{r^{ij}} - \frac{1}{2}\frac{\left(\epsilon_{\alpha\beta} r_\alpha^{ij} r_\beta^{ij}\right)^2}{(r^{ij})^3} + O(\epsilon^3). \tag{A13}$$

Considering the coefficient of first order term we get

$$\frac{\partial r_{ij}}{\partial \epsilon_{\alpha\beta}} = \frac{r_\alpha^{ij} r_\beta^{ij}}{r^{ij}}, \tag{A14}$$

and from the the second order term we have

$$\frac{\partial^2 U_{\mathrm{LJ}}}{\partial \epsilon_{\eta\nu}\partial \epsilon_{\alpha\beta}} = \frac{\partial}{\partial \epsilon_{\eta\nu}}\left(\frac{\partial \phi^{ij}}{\partial r_{ij}}\frac{\partial r_{ij}}{\partial \epsilon_{\alpha\beta}}\right) \tag{A15}$$

$$= \frac{\partial^2 \phi^{ij}}{\partial (r_{ij})^2}\frac{\partial r_{ij}}{\partial \epsilon_{\eta\nu}}\frac{\partial r_{ij}}{\partial \epsilon_{\alpha\beta}} + \frac{\partial \phi^{ij}}{\partial r_{ij}}\frac{\partial^2 r_{ij}}{\partial \epsilon_{\eta\nu}\partial \epsilon_{\alpha\beta}}. \tag{A16}$$

Using the aforementioned definition of the change in r^{ij} we obtain

$$\frac{\partial^2 r_{ij}}{\partial \epsilon_{\eta\nu}\partial \epsilon_{\alpha\beta}} = 2\frac{\left(r_\alpha^{ij}\right)^2\left(r_\beta^{ij}\right)^2}{(r^{ij})^3}. \tag{A17}$$

We now turn for the computation of the contribution in the shear modulus coming from the angular part of the potential ψ, which is

$$\frac{\partial \psi^\ell}{\partial \epsilon_{\alpha\beta}} = \frac{\partial \psi^\ell}{\partial \cos\varphi^\ell}\frac{\partial \cos\varphi^\ell}{\partial \epsilon_{\alpha\beta}}, \tag{A18}$$

$$\frac{\partial^2 \psi^\ell}{\partial \epsilon_{\eta\nu}\partial \epsilon_{\alpha\beta}} = \frac{\partial}{\partial \epsilon_{\eta\nu}}\left(\frac{\partial \psi^\ell}{\partial \cos\varphi^\ell}\frac{\partial \cos\varphi^\ell}{\partial \epsilon_{\alpha\beta}}\right)$$

$$= \frac{\partial^2 \psi^\ell}{\partial (\cos\varphi^\ell)^2}\frac{\partial \cos\varphi^\ell}{\partial \epsilon_{\eta\nu}}\frac{\partial \cos\varphi^\ell}{\partial \epsilon_{\alpha\beta}} + \frac{\partial \psi^\ell}{\partial \cos\varphi^\ell}\frac{\partial^2 \cos\varphi^\ell}{\partial \epsilon_{\eta\nu}\partial \epsilon_{\alpha\beta}}. \tag{A19}$$

The terms that remained to computed are

$$\frac{\partial \cos\varphi^\ell}{\partial \epsilon_{\alpha\beta}}.\frac{\partial^2 \cos\varphi^\ell}{\partial \epsilon_{\alpha\beta}\partial \epsilon_{\eta\nu}}. \tag{A20}$$

Using the definition of the cosine as

$$\cos\varphi^l = -\frac{r_\gamma^{l-1,l} r_\gamma^{l,l+1}}{r^{l-1,l} r^{l,l+1}}, \quad r_\gamma^{kl} = x_\gamma^l - x_\gamma^k,$$

we have

$$\frac{\partial \cos\varphi^l}{\partial \epsilon_{\alpha\beta}} = -\left[\frac{r_\gamma^{l,l+1}}{r^{l,l+1}}\frac{\partial}{\partial \epsilon_{\alpha\beta}}\left(\frac{r_\gamma^{l-1,l}}{r^{l-1,l}}\right) + \frac{r_\gamma^{l-1,l}}{r^{l-1,l}}\frac{\partial}{\partial \epsilon_{\alpha\beta}}\left(\frac{r_\gamma^{l,l+1}}{r^{l,l+1}}\right)\right],$$

$$\frac{\partial^2 \cos\varphi^l}{\partial \epsilon_{\eta\nu}\partial \epsilon_{\alpha\beta}} = -\left[\frac{r_\gamma^{l,l+1}}{r^{l,l+1}}\frac{\partial^2}{\partial \epsilon_{\eta\nu}\partial \epsilon_{\alpha\beta}}\left(\frac{r_\gamma^{l-1,l}}{r^{l-1,l}}\right) + \frac{r_\gamma^{l-1,l}}{r^{l-1,l}}\frac{\partial^2}{\partial \epsilon_{\eta\nu}\partial \epsilon_{\alpha\beta}}\left(\frac{r_\gamma^{l,l+1}}{r^{l,l+1}}\right)\right.$$

$$\left. + \frac{\partial}{\partial \epsilon_{\alpha\beta}}\left(\frac{r_\gamma^{l-1,l}}{r^{l-1,l}}\right)\frac{\partial}{\partial \epsilon_{\eta\nu}}\left(\frac{r_\gamma^{l,l+1}}{r^{l,l+1}}\right) + \frac{\partial}{\partial \epsilon_{\eta\nu}}\left(\frac{r_\gamma^{l-1,l}}{r^{l-1,l}}\right)\frac{\partial}{\partial \epsilon_{\alpha\beta}}\left(\frac{r_\gamma^{l,l+1}}{r^{l,l+1}}\right)\right],$$

where

$$\frac{\partial}{\partial \epsilon_{\alpha\beta}}\left(\frac{r_\gamma^{k\ell}}{r^{k\ell}}\right) = \frac{1}{r^{k\ell}}\frac{\partial r_\gamma^{k\ell}}{\partial \epsilon_{\alpha\beta}} - \frac{r_\gamma^{k\ell}}{(r^{k\ell})^2}\frac{\partial r^{k\ell}}{\partial \epsilon_{\alpha\beta}}$$

$$\frac{\partial^2}{\partial \epsilon_{\eta\nu}\partial \epsilon_{\alpha\beta}}\left(\frac{r_\gamma^{k\ell}}{r^{k\ell}}\right) = -\frac{1}{(r^{k\ell})^2}\frac{\partial r^{k\ell}}{\partial \epsilon_{\eta\nu}}\frac{\partial r_\gamma^{k\ell}}{\partial \epsilon_{\alpha\beta}} + \frac{1}{r^{k\ell}}\frac{\partial^2 r_\gamma^{k\ell}}{\partial \epsilon_{\eta\nu}\partial \epsilon_{\alpha\beta}} - \frac{1}{(r^{k\ell})^2}\frac{\partial r^{k\ell}}{\partial \epsilon_{\alpha\beta}}\frac{\partial r_\gamma^{k\ell}}{\partial \epsilon_{\eta\nu}} + \frac{2r_\gamma^{k\ell}}{(r^{k\ell})^3}\frac{\partial r^{k\ell}}{\partial \epsilon_{\eta\nu}}\frac{\partial r^{k\ell}}{\partial \epsilon_{\alpha\beta}} - \frac{r_\gamma^{k\ell}}{(r^{k\ell})^2}\frac{\partial^2 r^{k\ell}}{\partial \epsilon_{\eta\nu}\partial \epsilon_{\alpha\beta}}.$$

New derivatives that need to be defined are

$$\frac{\partial r_x^{k\ell}}{\partial \epsilon_{\alpha\beta}} = \begin{cases} 0; & \alpha = x, \beta = x \\ r_y^{k\ell}; & \alpha = x, \beta = y \\ r_y^{k\ell}; & \alpha = y, \beta = x \\ \approx 0; & \alpha = y, \beta = y \end{cases}, \tag{A21}$$

$$\frac{\partial r_y^{k\ell}}{\partial \epsilon_{\alpha\beta}} = 0, \tag{A22}$$

$$\frac{\partial^2 r_\gamma^{k\ell}}{\partial \epsilon_{\eta\nu} \partial \epsilon_{\alpha\beta}} = 0. \tag{A23}$$

Plugging the latter into cosine derivations we have

$$\frac{\partial \cos\varphi^\ell}{\partial \epsilon_{yy}} = -\left[\frac{r_\gamma^{\ell,\ell+1}}{r^{\ell,\ell+1}} \frac{\partial}{\partial \epsilon_{yy}}\left(\frac{r_\gamma^{\ell-1,\ell}}{r^{\ell-1,\ell}}\right) + \frac{r_\gamma^{\ell-1,\ell}}{r^{\ell-1,\ell}} \frac{\partial}{\partial \epsilon_{yy}}\left(\frac{r_\gamma^{\ell,\ell+1}}{r^{\ell,\ell+1}}\right)\right]$$

$$= -\left\{\frac{r_x^{\ell,\ell+1}}{r^{\ell,\ell+1}} \frac{\partial}{\partial \epsilon_{yy}}\left(\frac{r_x^{\ell-1,\ell}}{r^{\ell-1,\ell}}\right) + \frac{r_y^{\ell,\ell+1}}{r^{\ell,\ell+1}} \frac{\partial}{\partial \epsilon_{yy}}\left(\frac{r_y^{\ell-1,\ell}}{r^{\ell-1,\ell}}\right) + \frac{r_x^{\ell-1,\ell}}{r^{\ell-1,\ell}} \frac{\partial}{\partial \epsilon_{yy}}\left(\frac{r_x^{\ell,\ell+1}}{r^{\ell,\ell+1}}\right) + \frac{r_y^{\ell-1,\ell}}{r^{\ell-1,\ell}} \frac{\partial}{\partial \epsilon_{yy}}\left(\frac{r_y^{\ell,\ell+1}}{r^{\ell,\ell+1}}\right)\right\}$$

$$- \left\{\frac{r_x^{\ell,\ell+1}}{r^{\ell,\ell+1}}\left[-\frac{r_x^{\ell-1,\ell}\left(r_y^{\ell-1,\ell}\right)^2}{(r^{\ell-1,\ell})^3}\right] + \frac{r_y^{\ell,\ell+1}}{r^{\ell,\ell+1}}\left[-\frac{\left(r_y^{\ell-1,\ell}\right)^3}{(r^{\ell-1,\ell})^3}\right] + \frac{r_x^{\ell-1,\ell}}{r^{\ell-1,\ell}}\left[-\frac{r_x^{\ell,\ell+1}\left(r_y^{\ell,\ell+1}\right)^2}{(r^{\ell,\ell+1})^3}\right] + \frac{r_y^{\ell-1,\ell}}{r^{\ell-1,\ell}}\left[-\frac{\left(r_y^{\ell,\ell+1}\right)^3}{(r^{\ell,\ell+1})^3}\right]\right\}, \tag{A24}$$

$$\frac{\partial \cos\varphi^\ell}{\partial \epsilon_{xy}} = -\left[\frac{r_\gamma^{\ell,\ell+1}}{r^{\ell,\ell+1}} \frac{\partial}{\partial \epsilon_{xy}}\left(\frac{r_\gamma^{\ell-1,\ell}}{r^{\ell-1,\ell}}\right) + \frac{r_\gamma^{\ell-1,\ell}}{r^{\ell-1,\ell}} \frac{\partial}{\partial \epsilon_{xy}}\left(\frac{r_\gamma^{\ell,\ell+1}}{r^{\ell,\ell+1}}\right)\right] \tag{A25}$$

$$= -\left\{\frac{r_x^{\ell,\ell+1}}{r^{\ell,\ell+1}} \frac{\partial}{\partial \epsilon_{xy}}\left(\frac{r_x^{\ell-1,\ell}}{r^{\ell-1,\ell}}\right) + \frac{r_y^{\ell,\ell+1}}{r^{\ell,\ell+1}} \frac{\partial}{\partial \epsilon_{xy}}\left(\frac{r_y^{\ell-1,\ell}}{r^{\ell-1,\ell}}\right) + \frac{r_x^{\ell-1,\ell}}{r^{\ell-1,\ell}} \frac{\partial}{\partial \epsilon_{xy}}\left(\frac{r_x^{\ell,\ell+1}}{r^{\ell,\ell+1}}\right) + \frac{r_y^{\ell-1,\ell}}{r^{\ell-1,\ell}} \frac{\partial}{\partial \epsilon_{xy}}\left(\frac{r_y^{\ell,\ell+1}}{r^{\ell,\ell+1}}\right)\right\} \tag{A26}$$

$$= -\left\{\frac{r_x^{\ell,\ell+1}}{r^{\ell,\ell+1}}\left[\frac{2r_y^{\ell-1,\ell}}{r^{\ell-1,\ell}} - \frac{\left(r_x^{\ell-1,\ell}\right)^2 r_y^{\ell-1,\ell}}{(r^{\ell-1,\ell})^3}\right] + \frac{r_y^{\ell,\ell+1}}{r^{\ell,\ell+1}}\left[-\frac{r_x^{\ell-1,\ell}\left(r_y^{\ell-1,\ell}\right)^2}{(r^{\ell-1,\ell})^3}\right]\right.$$

$$\left. + \frac{r_x^{\ell-1,\ell}}{r^{\ell-1,\ell}}\left[\frac{2r_y^{\ell,\ell+1}}{r^{\ell,\ell+1}} - \frac{\left(r_x^{\ell,\ell+1}\right)^2 r_y^{\ell,\ell+1}}{(r^{\ell,\ell+1})^3}\right] + \frac{r_y^{\ell-1,\ell}}{r^{\ell-1,\ell}}\left[-\frac{r_x^{\ell,\ell+1}\left(r_y^{\ell,\ell+1}\right)^2}{(r^{\ell,\ell+1})^3}\right]\right\}, \tag{A27}$$

$$\frac{\partial^2 \cos\varphi^\ell}{\partial \epsilon_{xy} \partial \epsilon_{xy}} = -\left[\frac{r_\gamma^{\ell,\ell+1}}{r^{\ell,\ell+1}} \frac{\partial^2}{\partial \epsilon_{xy} \partial \epsilon_{xy}}\left(\frac{r_\gamma^{\ell-1,\ell}}{r^{\ell-1,\ell}}\right) + \frac{r_\gamma^{\ell-1,\ell}}{r^{\ell-1,\ell}} \frac{\partial^2}{\partial \epsilon_{xy} \partial \epsilon_{xy}}\left(\frac{r_\gamma^{\ell,\ell+1}}{r^{\ell,\ell+1}}\right) + 2\frac{\partial}{\partial \epsilon_{xy}}\left(\frac{r_\gamma^{\ell-1,\ell}}{r^{\ell-1,\ell}}\right)\frac{\partial}{\partial \epsilon_{xy}}\left(\frac{r_\gamma^{\ell,\ell+1}}{r^{\ell,\ell+1}}\right)\right] \tag{A28}$$

$$= -\left\{\frac{r_x^{\ell,\ell+1}}{r^{\ell,\ell+1}} \frac{\partial^2}{\partial \epsilon_{xy} \partial \epsilon_{xy}}\left(\frac{r_x^{\ell-1,\ell}}{r^{\ell-1,\ell}}\right) + \frac{r_y^{\ell,\ell+1}}{r^{\ell,\ell+1}} \frac{\partial^2}{\partial \epsilon_{xy} \partial \epsilon_{xy}}\left(\frac{r_y^{\ell-1,\ell}}{r^{\ell-1,\ell}}\right) + \frac{r_x^{\ell-1,\ell}}{r^{\ell-1,\ell}} \frac{\partial^2}{\partial \epsilon_{xy} \partial \epsilon_{xy}}\left(\frac{r_x^{\ell,\ell+1}}{r^{\ell,\ell+1}}\right)\right.$$

$$\left. + \frac{r_y^{\ell-1,\ell}}{r^{\ell-1,\ell}} \frac{\partial^2}{\partial \epsilon_{xy} \partial \epsilon_{xy}}\left(\frac{r_y^{\ell,\ell+1}}{r^{\ell,\ell+1}}\right) + 2\frac{\partial}{\partial \epsilon_{xy}}\left(\frac{r_x^{\ell-1,\ell}}{r^{\ell-1,\ell}}\right)\frac{\partial}{\partial \epsilon_{xy}}\left(\frac{r_x^{\ell,\ell+1}}{r^{\ell,\ell+1}}\right) + 2\frac{\partial}{\partial \epsilon_{xy}}\left(\frac{r_y^{\ell-1,\ell}}{r^{\ell-1,\ell}}\right)\frac{\partial}{\partial \epsilon_{xy}}\left(\frac{r_y^{\ell,\ell+1}}{r^{\ell,\ell+1}}\right)\right\} \tag{A29}$$

$$= -\left\{\frac{r_x^{\ell,\ell+1}}{r^{\ell,\ell+1}}\left[-2\frac{1}{(r^{\ell-1,\ell})^2}\frac{\partial r^{\ell-1,\ell}}{\partial \epsilon_{xy}}\frac{\partial r_x^{\ell-1,\ell}}{\partial \epsilon_{xy}} + 2\frac{r_x^{\ell-1,\ell}}{(r^{\ell-1,\ell})^3}\frac{\partial r^{\ell-1,\ell}}{\partial \epsilon_{xy}}\frac{\partial r^{\ell-1,\ell}}{\partial \epsilon_{xy}}\right] + \frac{r_y^{\ell,\ell+1}}{r^{\ell,\ell+1}}\left[2\frac{r_y^{\ell-1,\ell}}{(r^{\ell-1,\ell})^3}\frac{\partial r^{\ell-1,\ell}}{\partial \epsilon_{xy}}\frac{\partial r^{\ell-1,\ell}}{\partial \epsilon_{xy}}\right]\right.$$

$$+ \frac{r_x^{\ell-1,\ell}}{r^{\ell-1,\ell}}\left[-2\frac{1}{(r^{\ell,\ell+1})^2}\frac{\partial r^{\ell,\ell+1}}{\partial \epsilon_{xy}}\frac{\partial r_x^{\ell,\ell+1}}{\partial \epsilon_{xy}} + 2\frac{r_x^{\ell,\ell+1}}{(r^{\ell,\ell+1})^3}\frac{\partial r^{\ell,\ell+1}}{\partial \epsilon_{xy}}\frac{\partial r^{\ell,\ell+1}}{\partial \epsilon_{xy}}\right] + \frac{r_y^{\ell-1,\ell}}{r^{\ell-1,\ell}}\left[2\frac{r_y^{\ell,\ell+1}}{(r^{\ell,\ell+1})^3}\frac{\partial r^{\ell,\ell+1}}{\partial \epsilon_{xy}}\frac{\partial r^{\ell,\ell+1}}{\partial \epsilon_{xy}}\right]$$

$$+ 2\left[\frac{1}{r^{\ell-1,\ell}}\frac{\partial r_x^{\ell-1,\ell}}{\partial \epsilon_{xy}} - \frac{r_x^{\ell-1,\ell}}{(r^{\ell-1,\ell})^2}\frac{\partial r^{\ell-1,\ell}}{\partial \epsilon_{xy}}\right]\left[\frac{1}{r^{\ell,\ell+1}}\frac{\partial r_x^{\ell,\ell+1}}{\partial \epsilon_{xy}} - \frac{r_x^{\ell,\ell+1}}{(r^{\ell,\ell+1})^2}\frac{\partial r^{\ell,\ell+1}}{\partial \epsilon_{xy}}\right]$$

$$\left. + 2\left[\frac{1}{r^{\ell-1,\ell}}\frac{\partial r_y^{\ell-1,\ell}}{\partial \epsilon_{xy}} - \frac{r_y^{\ell-1,\ell}}{(r^{\ell-1,\ell})^2}\frac{\partial r^{\ell-1,\ell}}{\partial \epsilon_{xy}}\right]\left[\frac{1}{r^{\ell,\ell+1}}\frac{\partial r_y^{\ell,\ell+1}}{\partial \epsilon_{xy}} - \frac{r_y^{\ell,\ell+1}}{(r^{\ell,\ell+1})^2}\frac{\partial r^{\ell,\ell+1}}{\partial \epsilon_{xy}}\right]\right\} \tag{A30}$$

$$
\begin{aligned}
&= -\Bigg\{\frac{r_x^{\ell,\ell+1}}{r^{\ell,\ell+1}}\left(-\frac{4r_x^{\ell-1,\ell}\left(r_y^{\ell-1,\ell}\right)^2}{(r^{\ell-1,\ell})^4}+\frac{2\left(r_x^{\ell-1,\ell}\right)^3\left(r_y^{\ell-1,\ell}\right)^2}{(r^{\ell-1,\ell})^5}\right)+\frac{r_y^{\ell,\ell+1}}{r^{\ell,\ell+1}}\left(\frac{2\left(r_x^{\ell-1,\ell}\right)^2\left(r_y^{\ell-1,\ell}\right)^3}{(r^{\ell-1,\ell})^5}\right)\\
&\quad+\frac{r_x^{\ell-1,\ell}}{r^{\ell-1,\ell}}\left(-\frac{4r_x^{\ell,\ell+1}\left(r_y^{\ell,\ell+1}\right)^2}{(r^{\ell,\ell+1})^4}+\frac{2\left(r_x^{\ell,\ell+1}\right)^3\left(r_y^{\ell,\ell+1}\right)^2}{(r^{\ell,\ell+1})^5}\right)+\frac{r_y^{\ell-1,\ell}}{r^{\ell-1,\ell}}\left(\frac{2\left(r_x^{\ell,\ell+1}\right)^2\left(r_y^{\ell,\ell+1}\right)^3}{(r^{\ell,\ell+1})^5}\right)\\
&\quad+2\left(\frac{2r_y^{\ell-1,\ell}}{r^{\ell-1,\ell}}-\frac{\left(r_x^{\ell-1,\ell}\right)^2 r_y^{\ell-1,\ell}}{(r^{\ell-1,\ell})^3}\right)\left(\frac{2r_y^{\ell,\ell+1}}{r^{\ell,\ell+1}}-\frac{\left(r_x^{\ell,\ell+1}\right)^2 r_y^{\ell,\ell+1}}{(r^{\ell,\ell+1})^3}\right)+2\left(-\frac{r_x^{\ell-1,\ell}\left(r_y^{\ell-1,\ell}\right)^2}{(r^{\ell-1,\ell})^3}\right)\left(-\frac{r_x^{\ell,\ell+1}\left(r_y^{\ell,\ell+1}\right)^2}{(r^{\ell,\ell+1})^3}\right)\Bigg\}.
\end{aligned}
\tag{A31}
$$

For nonaffine forces = 0:

$$
\begin{aligned}
\frac{\partial^2\cos\varphi^\ell}{\partial x_\nu^m\partial\epsilon_{xy}} &= -\frac{\partial}{\partial\epsilon_{xy}}\Bigg\{(\delta^{\ell,m}-\delta^{\ell-1,m})\left[\frac{r_\nu^{\ell,l+1}}{r^{\ell,\ell+1}r^{\ell-1,\ell}}-\frac{r_\nu^{\ell-1,\ell}r_\gamma^{\ell-1,\ell}r_\gamma^{\ell,\ell+1}}{r^{\ell,\ell+1}(r^{\ell-1,\ell})^3}\right]+(\delta^{\ell+1,m}-\delta^{\ell,m})\left[\frac{r_\nu^{\ell-1,\ell}}{r^{\ell,\ell+1}r^{\ell-1,\ell}}-\frac{r_\nu^{\ell,\ell+1}r_\gamma^{\ell-1,\ell}r_\gamma^{\ell,\ell+1}}{r^{\ell-1,\ell}(r^{\ell,\ell+1})^3}\right]\Bigg\}\\
&= (\delta^{\ell-1,m}-\delta^{\ell,m})\left[\frac{\partial}{\partial\epsilon_{xy}}\frac{r_\nu^{\ell,l+1}}{r^{\ell,\ell+1}r^{\ell-1,\ell}}-\frac{\partial}{\partial\epsilon_{xy}}\frac{r_\nu^{\ell-1,\ell}r_\gamma^{\ell-1,\ell}r_\gamma^{\ell,\ell+1}}{r^{\ell,\ell+1}(r^{\ell-1,\ell})^3}\right]\\
&\quad+(\delta^{\ell,m}-\delta^{\ell+1,m})\left[\frac{\partial}{\partial\epsilon_{xy}}\frac{r_\nu^{\ell-1,\ell}}{r^{\ell,\ell+1}r^{\ell-1,\ell}}-\frac{\partial}{\partial\epsilon_{xy}}\frac{r_\nu^{\ell,\ell+1}r_\gamma^{\ell-1,\ell}r_\gamma^{\ell,\ell+1}}{r^{\ell-1,\ell}(r^{\ell,\ell+1})^3}\right]\\
&= (\delta^{\ell-1,m}-\delta^{\ell,m})\left[\frac{1}{r^{\ell-1,\ell}}\frac{\partial}{\partial\epsilon_{xy}}\frac{r_\nu^{\ell,l+1}}{r^{\ell,\ell+1}}+\frac{r_\nu^{\ell,l+1}}{r^{\ell,\ell+1}}\frac{\partial}{\partial\epsilon_{xy}}\frac{1}{r^{\ell-1,\ell}}-\frac{r_\nu^{\ell-1,\ell}r_\gamma^{\ell-1,\ell}}{(r^{\ell-1,\ell})^3}\frac{\partial}{\partial\epsilon_{xy}}\frac{r_\gamma^{\ell,\ell+1}}{r^{\ell,\ell+1}}-\frac{r_\gamma^{\ell,\ell+1}}{r^{\ell,\ell+1}}\frac{\partial}{\partial\epsilon_{xy}}\frac{r_\nu^{\ell-1,\ell}r_\gamma^{\ell-1,\ell}}{(r^{\ell-1,\ell})^3}\right]\\
&\quad+(\delta^{\ell,m}-\delta^{\ell+1,m})\left[\frac{1}{r^{\ell,\ell+1}}\frac{\partial}{\partial\epsilon_{xy}}\frac{r_\nu^{\ell-1,\ell}}{r^{\ell-1,\ell}}+\frac{r_\nu^{\ell-1,\ell}}{r^{\ell-1,\ell}}\frac{\partial}{\partial\epsilon_{xy}}\frac{1}{r^{\ell,\ell+1}}-\frac{r_\nu^{\ell,\ell+1}r_\gamma^{\ell,\ell+1}}{(r^{\ell,\ell+1})^3}\frac{\partial}{\partial\epsilon_{xy}}\frac{r_\gamma^{\ell-1,\ell}}{r^{\ell-1,\ell}}-\frac{r_\gamma^{\ell-1,\ell}}{r^{\ell-1,\ell}}\frac{\partial}{\partial\epsilon_{xy}}\frac{r_\nu^{\ell,\ell+1}r_\gamma^{\ell,\ell+1}}{(r^{\ell,\ell+1})^3}\right].
\end{aligned}
\tag{A32}
$$

Using previously defined expressions and

$$
\frac{\partial}{\partial\epsilon_{\alpha\beta}}\frac{r_\nu^{k\ell}r_\gamma^{k\ell}}{(r^{k\ell})^3}=\frac{r_\gamma^{k\ell}}{(r^{k\ell})^3}\frac{\partial r_\nu^{k\ell}}{\partial\epsilon_{\alpha\beta}}+\frac{r_\nu^{k\ell}}{(r^{k\ell})^3}\frac{\partial r_\gamma^{k\ell}}{\partial\epsilon_{\alpha\beta}}-\frac{3r_\nu^{k\ell}r_\gamma^{k\ell}}{(r^{k\ell})^4}\frac{\partial r^{k\ell}}{\partial\epsilon_{\alpha\beta}}
\tag{A33}
$$

we have the final expression of the second derivative of cosine as

$$
\begin{aligned}
\frac{\partial^2\cos\varphi^\ell}{\partial x_\nu^m\partial\epsilon_{xy}} &= (\delta^{\ell-1,m}-\delta^{\ell,m})\Bigg\{\frac{1}{r^{\ell-1,\ell}}\left[\frac{\delta^{\nu x}2r_y^{\ell,\ell+1}}{r^{\ell,\ell+1}}-\frac{r_\nu^{\ell,\ell+1}r_x^{\ell,\ell+1}r_y^{\ell,\ell+1}}{(r^{\ell,\ell+1})^3}\right]-\frac{r_\nu^{\ell,l+1}}{r^{\ell,\ell+1}}\left[\frac{r_x^{\ell-1,\ell}r_y^{\ell-1,\ell}}{(r^{\ell-1,\ell})^3}\right]\\
&\quad-\frac{r_\nu^{\ell-1,\ell}r_\gamma^{\ell-1,\ell}}{(r^{\ell-1,\ell})^3}\left[\frac{2r_y^{\ell,l+1}}{r^{\ell,\ell+1}}-\frac{r_\gamma^{\ell,l+1}r_x^{\ell,l+1}r_y^{\ell,l+1}}{(r^{\ell,\ell+1})^3}\right]\\
&\quad-\frac{r_\gamma^{\ell,\ell+1}}{r^{\ell,\ell+1}}\left[\frac{2r_y^{\ell-1,\ell}\left(\delta^{\nu x}r_\gamma^{\ell-1,\ell}+r_\nu^{\ell-1,\ell}\right)}{(r^{\ell-1,\ell})^3}-\frac{3r_\gamma^{\ell-1,\ell}r_\nu^{\ell-1,\ell}r_x^{\ell-1,\ell}r_y^{\ell-1,\ell}}{(r^{\ell-1,\ell})^5}\right]\Bigg\}\\
&\quad+(\delta^{\ell,m}-\delta^{\ell+1,m})\Bigg\{\frac{1}{r^{\ell,\ell+1}}\left[\frac{\delta^{\nu x}2r_y^{\ell-1,\ell}}{r^{\ell-1,\ell}}-\frac{r_\nu^{\ell-1,\ell}r_x^{\ell-1,\ell}r_y^{\ell-1,\ell}}{(r^{\ell-1,\ell})^3}\right]+\frac{r_\nu^{\ell-1,\ell}}{r^{\ell-1,\ell}}\left[\frac{r_x^{\ell,\ell+1}r_y^{\ell,\ell+1}}{(r^{\ell,\ell+1})^3}\right]\\
&\quad-\frac{r_\nu^{\ell,\ell+1}r_\gamma^{\ell,\ell+1}}{(r^{\ell,\ell+1})^3}\left[\frac{2r_y^{\ell-1,\ell}}{r^{\ell-1,\ell}}-\frac{r_\nu^{\ell-1,\ell}r_x^{\ell-1,\ell}r_y^{\ell-1,\ell}}{(r^{\ell-1,\ell})^3}\right]\\
&\quad-\frac{r_\gamma^{\ell-1,\ell}}{r^{\ell-1,\ell}}\left[\frac{2r_y^{\ell,\ell+1}\left(\delta^{\nu x}r_\gamma^{\ell,\ell+1}+r_\nu^{\ell,\ell+1}\right)}{(r^{\ell,\ell+1})^3}-\frac{3r_\gamma^{\ell,\ell+1}r_\nu^{\ell,\ell+1}r_x^{\ell,\ell+1}r_y^{\ell,\ell+1}}{(r^{\ell,\ell+1})^5}\right]\Bigg\}.
\end{aligned}
\tag{A34}
$$

[1] M. Rubinstein and R. H. Colby, *Polymer Physics* (Oxford University Press, Oxford, 2003).

[2] A. M. Donald and E. J. Kramer, J. Materials Sci. **17**, 1765 (1982).

[3] P. H. Mott, A. S. Argon, and U. W. Suter, Phil. Magazine A **67**, 931 (1993).

[4] M. Warren and J. Rottler, Phys. Rev. E **76**, 031802 (2007).

[5] F. Varnik, L. Bocquet, and J.-L. Barrat, J. Chem. Phys. **120**, 2788 (2004).
[6] A. Makke, M. Perez, J. Rottler, O. Lame, and J. L. Barrat, Macromol. Theory Simul. **20**, 826 (2011).
[7] R. S. Hoy and M. O. Robbins, Phys. Rev. Lett. **99**, 117801 (2007); Phys. Rev. E **77**, 031801 (2008).
[8] J. L. Barrat, J. Baschnagel, and A. Lyulin, Soft Matter **6**, 3430 (2010).
[9] D. L. Malandro and D. J. Lacks, J. Chem. Phys. **110**, 4593 (1999); Comp. Theor. Polymer Sci. **9**, 353 (1999).
[10] C. E. Maloney and A. Lemaître, Phys. Rev. E **74**, 016118 (2006).
[11] E. Lerner and I. Procaccia, Phys. Rev. E **79**, 066109 (2009).
[12] R. Dasgupta, H. G. E. Hentschel, and I. Procaccia, Phys. Rev. Lett. **109**, 255502 (2012); Phys. Rev. E **87**, 022810 (2013).
[13] R. Dasgupta, O. Gendelman, P. Mishra, I. Procaccia, and C. A. B. Z. Shor, Phys. Rev. E **88**, 032401 (2013).
[14] H. G. E. Hentschel, V. Ilyin, and I. Procaccia, Europhys. Lett. **99**, 26003 (2012).
[15] R. Dasgupta, H. G. E. Hentschel, I. Procaccia, and B. Sen Gupta, Europhys. Lett. **104**, 47003 (2013).
[16] H. G. E. Hentschel, V. Iliyn, I. Procaccia, and B. Sen Gupta, J. Stat. Mech. (2014) P08020.
[17] K. Binder, J. Baschnagel, and W. Paul, Prog. Polymer Sci. **28**, 115 (2003).
[18] K. Kramer and G. S. Grest, J. Chem. Phys. **92**, 5057 (1990).
[19] R. Auhl, R. Everaers, G. S. Grest, K. Kremer, and S. J. Plimpton, J. Chem. Phys. **119**, 12718 (2003).
[20] P. G. De Gennes, J. Chem. Phys. **60**, 5030 (1974).
[21] J. Ashwin, O. Gendelman, I. Procaccia, and C. Shor, Phys. Rev. E **88**, 022310 (2013).
[22] S. Karmakar, E. Lerner, and I. Procaccia, Phys. Rev. E **82**, 026105 (2010). For a fuller detailed exposition see arXiv:1004.2198.
[23] M. L. Falk and J. S. Langer, Annu. Rev. Condens. Matt. Phys. **2**, 353 (2011).
[24] S. M. Fielding, P. Sollich, and M. E. Cates, J. Rheol. **44**, 323 (2000).